Journal of Materials Science: Materials in Electronics (2018) 29:12735–12743
https://doi.org/10.1007/s10854-018-9391-7

Determining electrical and dielectric parameters of Al/ZnS-PVA/p-Si (MPS) structures in wide range of temperature and voltage

Nalan Baraz[1] · İbrahim Yücedağ[2] · Yashar Azizian-Kalandaragh[3,4] · Şemsettin Altındal[5]

Received: 8 February 2018 / Accepted: 31 May 2018 / Published online: 16 June 2018
© Springer Science+Business Media, LLC, part of Springer Nature 2018

Abstract

In this study zinc sulphide (ZnS) nanostructures have been prepared by microwave-assisted method in presence of polyvinyl alcohol (PVA) as a capping agent. The structural and morphological properties of prepared sample have been investigated by X-ray diffraction (XRD) and scanning electron microscopy (SEM). These analyses confirm that the sample has nano structure. They have been used this sample to fabrication of Al/ZnS-PVA/p-Si structure. The effect of temperature and voltage on the electrical and dielectric parameters of the Al/ZnS-PVA/p-Si (MPS) structures has been investigated in the wide range of temperature (140–340 K) and voltage (− 2 V to + 4 V) using capacitance/conductance-voltage (*C/G–V)* measurements at 500 kHz. Experimental measurements revealed that the values of *C/G–V* increase with increasing temperature but the values of series resistance (R_s) increase with decreasing temperature. As well as the dielectric parameters such as the values of real and imaginary parts of the dielectric constants (ε' and ε'') and electric modules (M' and M''), loss tangent ($tan\delta$), and ac electrical conductivity (σ_{ac}) were obtained using C and G/ω data. These parameters are found out as strong functions of temperature and voltage. While the values of ε', ε'' and tanδ increase with increasing temperature, the values of σ_{ac}, M' and M'' decrease. The Arrhenius plot (ln(σ_{ac}) vs q/kT) shows two distinct linear ranges with different slopes or activation energies (E_a) at low (140–230 K) and high (260–340 K) temperatures. Both values of R_s and (ZnS-PVA) interfacial layers are also very effective parameters on the electric and dielectric properties.

1 Introduction

The polymeric materials fabricated on semiconductors play a significant role in the description of the characteristic parameters of the metal-polymer-semiconductor (MPS) devices. Researchers have paid so much attention to the fabrication and electrical characterization of metal–insulator/polymer–semiconductor (MIS/MPS) devices such as Schottky barrier diodes (SBDs), transistors, p–n junctions, and solar cells [1–7]. The sample temperature and applied bias voltage are two important parameters on the conduction mechanism, electrical and dielectric properties of these devices. It is well known that the electrical measurements at one point or in the narrow ranges of the temperature and voltage cannot provide sufficient information to us about conduction mechanism and main electrical and dielectric parameters of the devices.

In addition, both electrical and dielectric properties of these devices are influenced by various non-idealities such as series resistance (R_s) [1, 8, 9], interface layer and surface states [10–12]. Some polymers can be preferred owing to their electrical, dielectric and physical properties over a wide range of temperature and frequencies because their optical and electrical properties are very suitable in the devices aimed to be fabricated.

Among various polymers, poly (vinyl alcohol) (PVA), as one of the most important polymers, has received considerable interest because of its unique chemical and physical properties as well as its industrial applications [4, 10, 13]. In addition, polyvinyl alcohol is a potential material having a very high dielectric strength

✉ Nalan Baraz
nalanbaraz@gmail.com

[1] Department of Electric and Energy, Gölyaka Vocational High School, Düzce University, 81800 Düzce, Turkey

[2] Department of Computer Engineering, Technology Faculty, Düzce University, 81620 Düzce, Turkey

[3] Department of Physics, University of Mohaghegh Ardabili, P.O. Box 179, Ardabil, Iran

[4] Department of Engineering Sciences, Sabalan University of Advanced Technologies (SUAT), Namin, Iran

[5] Department of Physics, Faculty of Sciences, Gazi University, Ankara, Turkey

(> 1000 kV/mm), good charge storage capacity and dopant-dependent electrical and optical properties [14]. Zinc sulphide (ZnS) is one of the most important group II-VI semiconductors with direct wide band gap about 3.7 eV at ambient temperature with many excellent chemical and physical properties which has promising applications in a lot of technical fields including electroluminescence, field effect transistors, light-emitting diodes, catalysis, sensors [15] and so on. It has low absorption coefficient in the visible range of optical spectrum and good electrical properties. Many methods such as solvothermal, chemical bath deposition, hydrothermal, thermal evaporation, sonochemical, wet chemical process, solid state, micro-emulsion, microwave irradiation have been developed for preparation of ZnS nanomaterials [16–18]. Among these synthesis methods, the microwave assisted method has proven to be a simple method for the production of nanomaterials. Compared with the conventional methods, the microwave synthesis has the advantages of a short reaction time, small particle size, narrow particle size distribution, and high purity [19, 20].

In the previous study [21], both electrical and dielectric properties of the fabricated Al/(ZnS-PVA)/p-Si (MPS) structures have been investigated as function of frequency and voltage by using *C–V* and *G/ω–V* measurements in wide range of frequencies 10 kHz–5 MHz at room temperature and we found that the values of ε', ε'', and $tan\delta$ increase with increasing frequency, whereas M' and σ_{ac} decrease. The changes in these parameters with temperature are also more important with temperature and applied bias voltage. Therefore, in this study, we aimed that the characterization and investigation of the electrical and dielectric properties of the fabricated Al/(ZnS-PVA)/p-Si (MPS) type structures both in the wide range of temperature and voltage at 500 kHz. Experimental results confirmed that these parameters are considerably as function of temperature and applied bias voltage especially in depletion and accumulation regions due to the existence of interfacial polymer layer and surface states between metal and semiconductor and series resistance of the structure. While the values of ε', ε'' and $tan\delta$ increase with increasing temperature, the values of σ_{ac}, M' and M'' decrease. The Arrhenius plot ($ln(\sigma_{ac})$ vs. q/kT) shows two distinct linear ranges with different slopes or activation energies (E_a) at low (140–200 K) and high (230–340 K) temperatures. Both values of R_s and (ZnS-PVA) interfacial layers are also very effective parameters on the electric and dielectric properties.

2 Materials and methods

2.1 Preparation of polyvinyl alcohol (PVA) stabilized ZnS nanostructures

Zinc acetate ($(CH_3CO_2)2\ Zn\cdot 2H_2O$), sodium sulphide ($Na_2S\cdot 9H_2O$), polyvinyl alcohol (PVA $(C_2H_4O)_x$) powder and absolute ethanol were obtained from Merck and directly employed without purification. PVA-Capped ZnS nanostructures were prepared using the following typical procedure: 0.87 g $(CH_3CO_2)2\ Zn\cdot 2H_2O$ (0.2 M) and 0.48 g $Na_2S\cdot 9H_2O$ (0.1 M) were dissolved in 20 mL distilled water and 1 mL PVA (5%) was added to mixture solution. Then the solution was placed into a homemade microwave oven (model: LG, 600 W) and was heated under microwave irradiation for five minutes under a refluxing system. The prepared suspension was centrifuged to get the precipitate out and washed four times using double distilled water and ethanol to remove the unreacted reagents and dried in an oven at 80 °C for 3 h.

2.2 Fabrication of Al/PVA-ZnS/p-Si structure

Al/ZnS-PVA/p-Si (MPS) type structures were fabricated on N-doped (p-Si) single Si wafer with (100) orientation, ~ 300 µm thickness and 1–10 Ω cm resistivity. The structure of Al/ZnS-PVA/p-Si structure and the details of its fabrication processes have been given in our previous study [21].

2.3 Instrument

The structural characterization of nanocrystals was carried out by analyzing X-ray diffraction (XRD) patterns, obtained using a Philips X'Pert, X-ray diffractometer using CuKa radiation (wavelength = 1.54056 Å). The surface morphology of samples was analyzed using a scanning electron microscope (SEM), LEO, 1430VP at 15 kV accelerating voltage. The capacitance–voltage (C–V) and the conductance voltage (G/ω–V) measurements of the Al/ZnS-PVA/p-Si (MPS) type structures were performed in the temperature range of 140–340 K at 500 kHz using an HP 4192A LF impedance analyzer (5 Hz–13 MHz) and a test signal of 50 mV peak to peak. All measurements were carried out in a Janes vpf-475 cryostat, which enabled us to make measurements in the temperature range of 77–450 K. The samples, temperatures were controlled by using a Lake Shore model 321 auto-tuning temperature controller with sensitivity better than ± 0.1 K. In addition, all measurements were carried out with the help of a microcomputer with an IEEE-488 ac/dc converter card.

3 Results and discussion

3.1 Stractural and morphological analysis

3.1.1 XRD

Figure 1 shows the XRD pattern of ZnS-PVA nanostructure prepared by microwave-assisted method. No additional peaks were observed, but the intensity of peaks is low and the peaks are relatively noisy. As can be seen in Fig. 1, the observed three different diffraction (111), (220) and (311) peaks are corresponding to the cubic crystalline ZnS with cubic structure (*JCPDS* Data file: 05-0566-cubic). On the other hand, the relatively noisy behavior of the XRD pattern indicates the existence of the amorphous PVA materials inside the structure.

The mean crystallite size of ZnS-PVA nanostructures was calculated using Debye–Scherer's equation:

$$D = 0.9\lambda/\beta\cos\theta \tag{1}$$

In Eq. (1), D is the average crystalline size, λ is the wavelength of Cu Kα, β is the full width at half maximum of the diffraction peak and θ is the Bragg's angle [22]. Table 1 shows the list of peaks, their position and the size of crystal.

The estimated nanostructure size using Debye–Scherer's equation show that nano-crystallite size of prepared sample is below the 35 nm and the mean nano-crystallite size is 30 nm.

3.1.2 SEM analysis

Figure 2 shows the scanning electron microscopy of ZnS-PVA nanostructure prepared by microwave-assisted method.

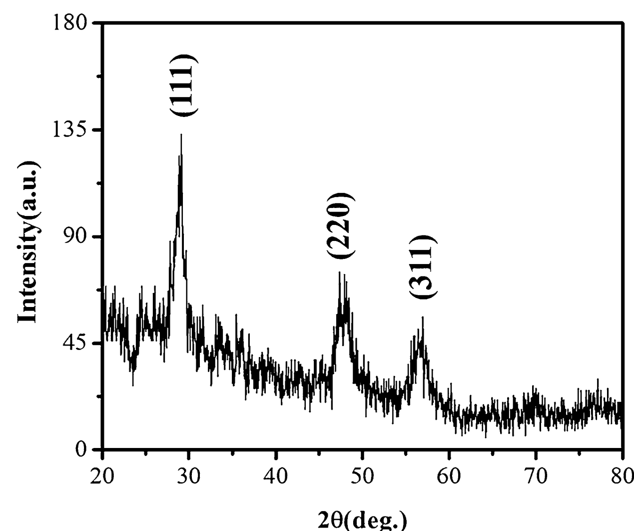

Fig. 1 XRD pattern of ZnS-PVA sample

Table 1 Peaks position and their size

Peak (Miller Indices)	Position (2θ)	Crystal size (nm)
111	28.6524	29
220	48.3290	34
311	57.4539	27

The SEM image show that the particles of ZnS-PVA sample are in nano scale and have uniform spherical shape.

3.2 Electrical and dielectric properties

The *C–V* and *G/ω–V* measurements of semiconductor devices such as MPS, MIS or MOS type structures must be wide range of the temperature. It is well known that the electrical measurements at one point or in the narrow ranges of the temperature and voltage cannot provide sufficient information to us about conduction mechanism and main electrical and dielectric parameters of the devices. Therefore, in this study, the *C–V* and *G/ω–V* measurements of the Al/ZnS-PVA/p-Si (MPS) structures have been measured in the wide temperature range (140–340 K) at 500 kHz frequency and are given in Fig. 3a, b, respectively. Because at sufficiently high frequencies ($f \geq 500$ kHz), interface states (N_{ss}) cannot follow the ac signal [23–27]. In other words, the effect of N_{ss} can be neglected low and so cannot any contribution to the measured of *C* and *G* values. But the value of R_s is effective on the *C–V* and *G/ω–V* plots especially at accumulation region. As shown in Fig. 3a, b, both *C–V* and *G/ω–V* characteristics exhibit accumulation, depletion and inversion regions. It is clear that both values of *C* and *G/ω* increase with increasing temperature in the whole measured range.

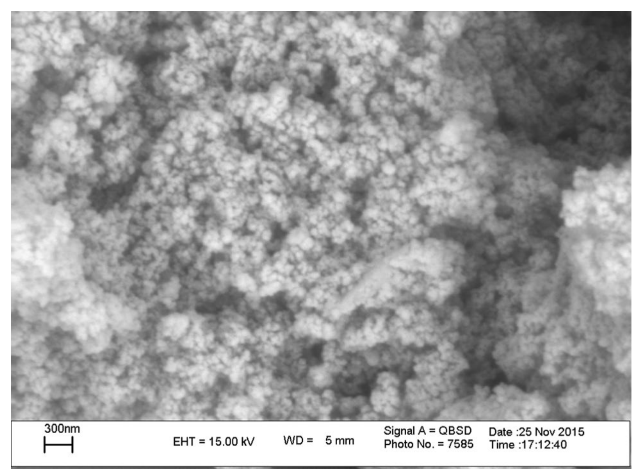

Fig. 2 SEM image of ZnS-PVA sample

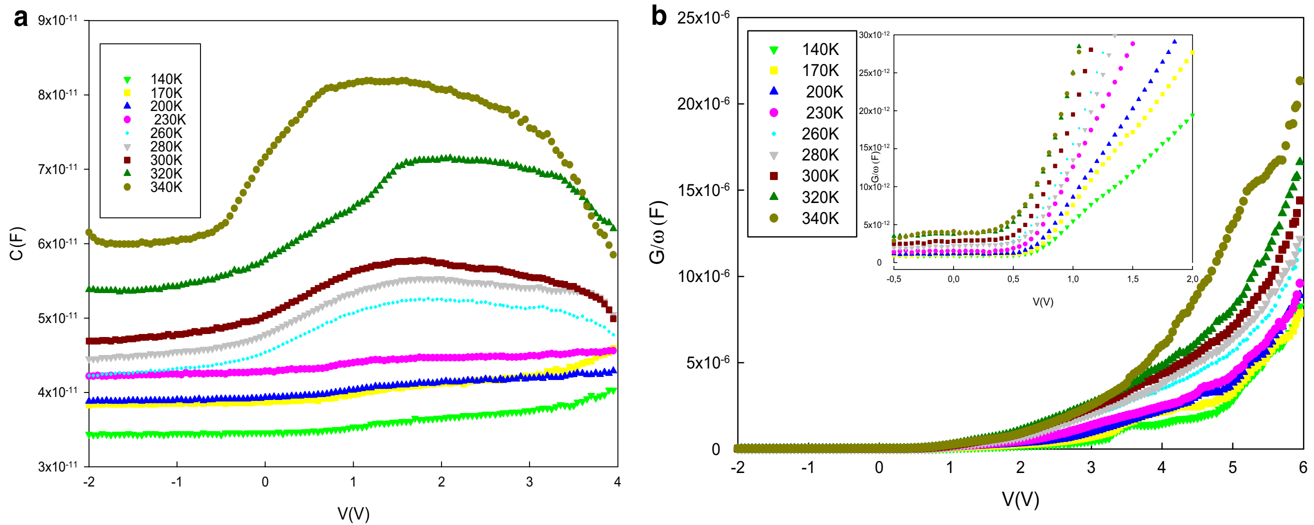

Fig. 3 Capacitance–voltage (*C–V*) (**a**) and conductance–voltage (*G/ω–V*) (**b**) plots of the Al/ZnS-PVA/p-Si (MPS) structure at various temperatures and at 500 kHz

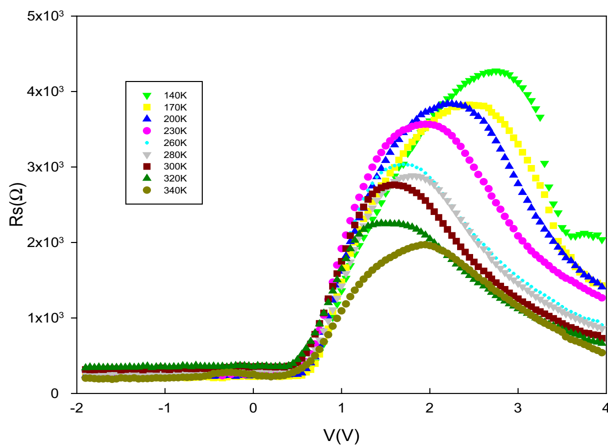

Fig. 4 R_s–*V* plots of the Al/ZnS-PVA/p-Si (MPS) structure at various temperatures at 500 kHz

As explained above, the R_s of the diode is important parameters which are more effective on the *C–V* and *G/ω–V* characteristics. Therefore, the calculation of R_s as a function of temperature and voltage is more important. Thus, the voltage dependent profile of R_s was calculated according to Eq. (2) for each temperature and is given in Fig. 4 for each temperature.

$$R_S = \frac{G_m}{G_m^2 + (\omega C_m)^2} \tag{2}$$

But the reel value of R_s is corresponding to the strong accumulation region at enough high frequencies (f ≥ 500 kHz) according to Nicollian and Brews [28]. As seen in Fig. 4, the R_s versus *V* plots give a peak for each temperature and peak position shifts toward negative bias region with increasing temperature and the magnitudes of the peak decrease with increasing temperature, indicating that the trap charges need less energy to escape from traps at high temperatures.

It is well known both the electrical characteristics and dielectric properties of the MS structure with and without an interfacial insulator or polymer layer are strong depended on temperature and voltage. Therefore, the main dielectric parameters such as ε', ε'', tanδ, M', M' and σ_{ac} of the Al/ZnS-PVA/p-Si (MPS) structures have been also investigated using the measured *C* and *G* data in the wide range of temperature and voltage. Firstly, the ε' and ε'' values of were obtained by using the following formulas and are given in Figs. 5, 6, respectively.

$$\varepsilon = \varepsilon' - j\varepsilon'' = \frac{Cd}{A\varepsilon_o} - j\left(\frac{Gd}{\omega A\varepsilon_o}\right) \tag{3}$$

where *j* is the imaginary root of −1, *C* and *G* are the measured capacitance and conductance of the dielectric, *A* is rectifier contact area (7.85×10^{-3} cm^2), *d* is the thickness of the interfacial ZnS-PVA layer (500 Å), $\varepsilon_o = 8.85\times10^{-14}$ F/cm is the permittivity of the vacuum.

As shown in Figs. 5 and 6, both values of ε' and ε'' increase with increasing temperature especially in depletion and accumulation regions due to reordering and restructure under electric field and temperature. The rate of increase, as the temperature causes a loosening of the rigid structure, resulted from an increase in the dipole

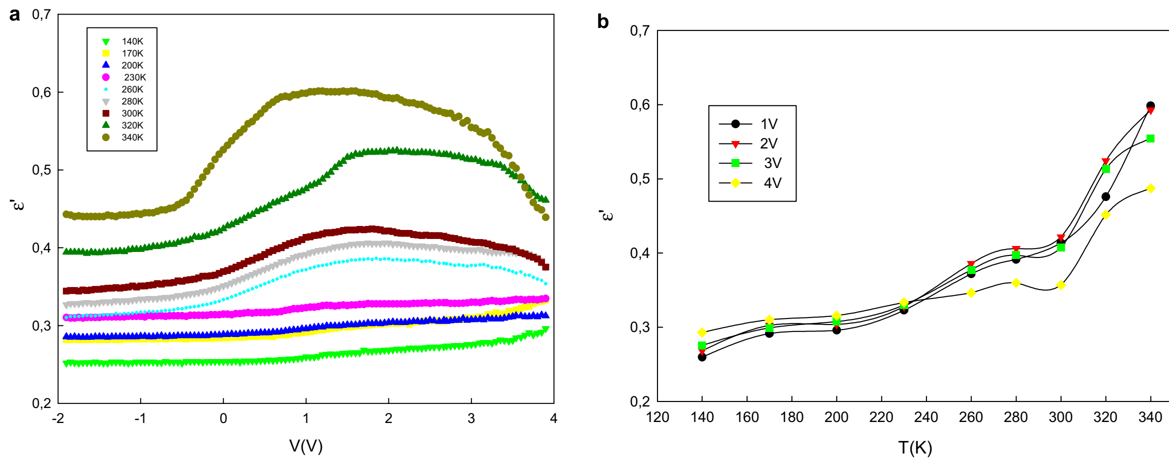

Fig. 5 **a** ε'–V and **b** ε'–T plots of the Al/ZnS-PVA/p-Si (MPS) structure

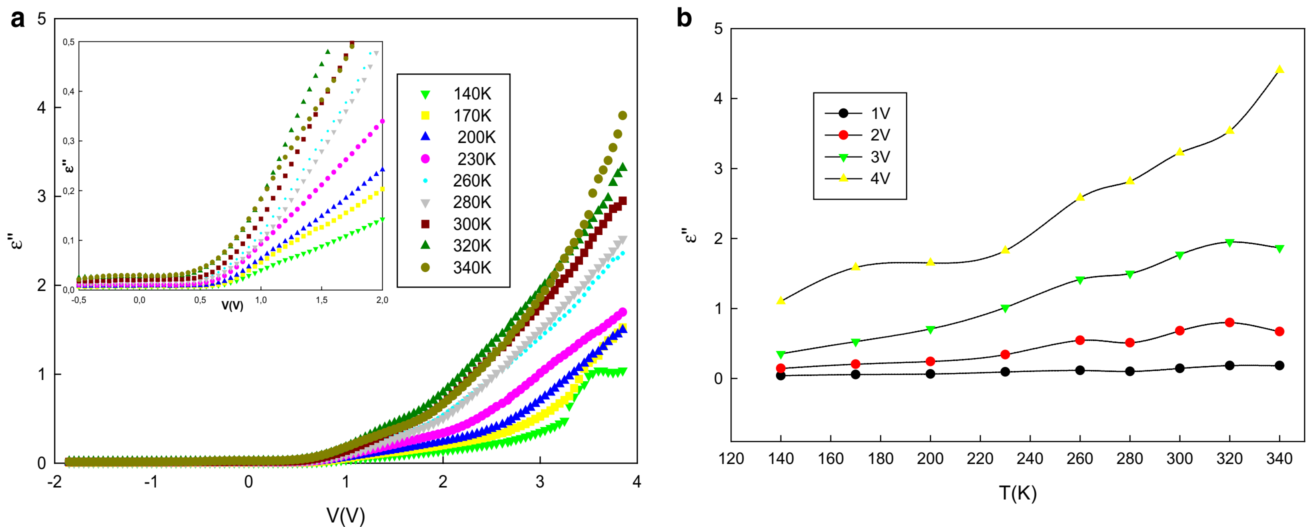

Fig. 6 **a** ε''–V and **b** ε''–T plots of the Al/ZnS-PVA/p-Si (MPS) structure

orientation and, hence, an increase in ε' [24]. It is clear that both the values of ε' and ε'' are strong function of temperature and voltage at 500 kHz. While the value of *C* decrease in the strong accumulation region, the value of *G* stars to increase. Such behavior of *C* and *G* is called inductive behavior. In other words, the minimum value of *C* is corresponding to *G* for each temperature.

The value of loss tangent (tanδ) can be extracted from as following equation

$$\tan\delta = \frac{\varepsilon''}{\varepsilon'} \tag{4}$$

The voltage and temperature dependent profile of tanδ was calculated from Eq. (4) and given in Fig. 7. As shown in Fig. 7a, b, the value of tanδ decrease with increasing temperature and they remain constant in the inversion region (at negative bias voltage). The increase in electrical conductivity (σ_{ac}) leads to increase in the eddy current which in turn increases the energy loss tangent.

The complex dielectric constant ($\varepsilon^* = 1/M^*$) data are changed into the complex electric modulus formula ($M^* = M' + jM''$). Thus real (M') and the imaginary component (M'') of M^* were calculated from ε' and ε'' by using Eq. (5) and are presented in Fig. 8a, b, respectively.

$$M^* = \frac{1}{\varepsilon^*} = M' + jM'' = \frac{\varepsilon'}{\varepsilon'^2 + \varepsilon''^2} + j\frac{\varepsilon''}{\varepsilon'^2 + \varepsilon''^2} \tag{5}$$

As can be seen in Figs. 7 and 8 the values of M' and M'' were also found to be a strong function of temperature and voltage. The values of M' and M'' reach a maximum constant

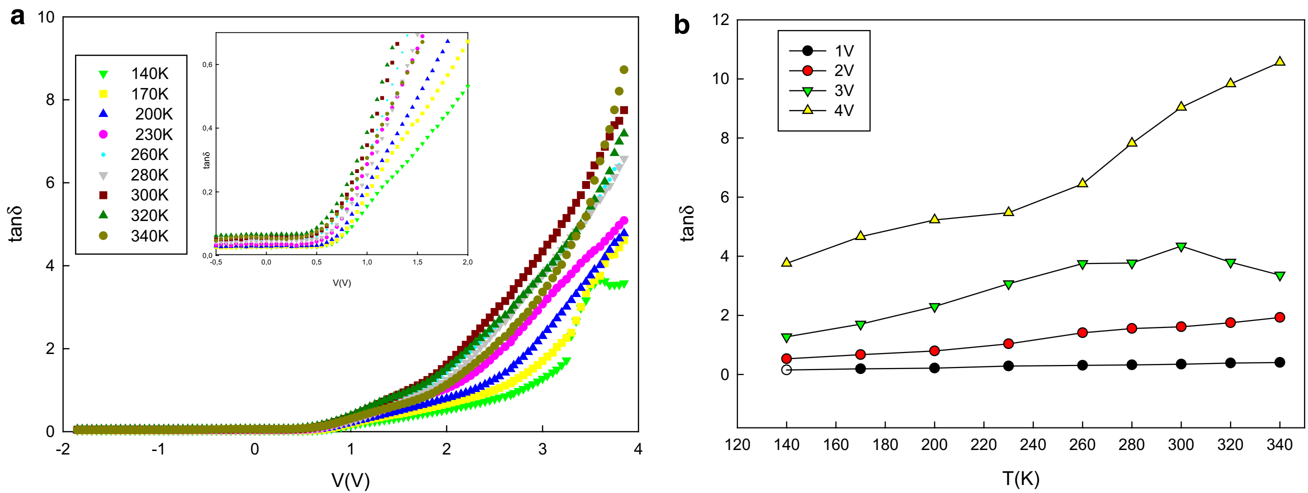

Fig. 7 **a** tanδ–V and **b** tanδ–T plots of the tanδ for the Al/ZnS-PVA/p-Si (MPS) structure

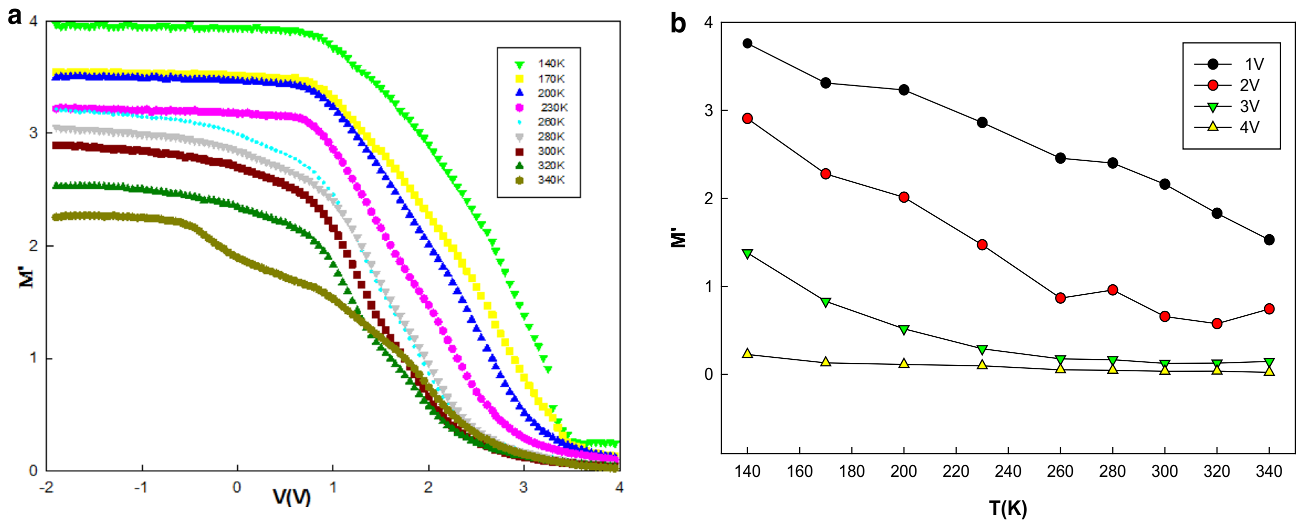

Fig. 8 **a** M'–V and **b** M'–T plots of the Al/ZnS-PVA/p-Si (MPS) structure

value corresponding to $M_\infty \approx 1/\varepsilon_\infty$ due to the relaxation process. It is clear that the value of M' decreases with increasing temperature and voltage, whereas M'' gives a peak for each temperature (Fig. 9a, b).

The temperature region below the peak frequency of M″ versus frequency spectra determines the range in which charge carriers are mobile over long distances [25, 29–33].

The AC electrical conductivity (σ_{ac}) of the structures was obtained from the following equation and given in Fig. 10.

$$\sigma_{ac} = 2\pi f \varepsilon_o \varepsilon' \tan\delta \tag{6}$$

Figure 10 shows the temperature dependence of the ac electrical conductivity of the Al/ZnS-PVA/p-Si (MPS) structures. It is clear that the value of σ_{ac} increases with increasing temperature. The increases in the electrical conductivity at high temperatures are attributed to the impurities or dislocations which reside at the grain boundaries [34–36].

$$\sigma_{ac} = \sigma_0 \, exp\left(-\frac{qE_a}{kT}\right) \tag{7}$$

Figure 11 is illustrating the Arrhenius plot of the ac conductivity at 500 kHz. As can be seen in Fig. 11, *ln(σac)* versus q/kT plot for the structure has two distinct linear regions with different slopes. Such behavior of these plots confirmed the existence of two different conduction mechanisms which correspond to the low and high

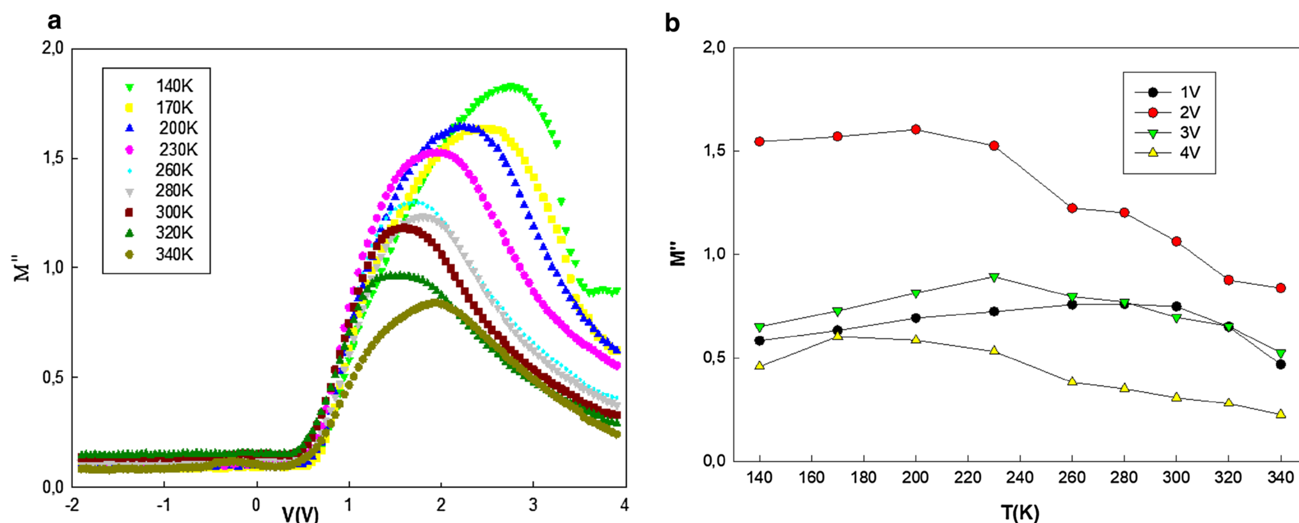

Fig. 9 **a** M''–V and **b** M''–T plots of the Al/ZnS-PVA/p-Si (MPS) structure

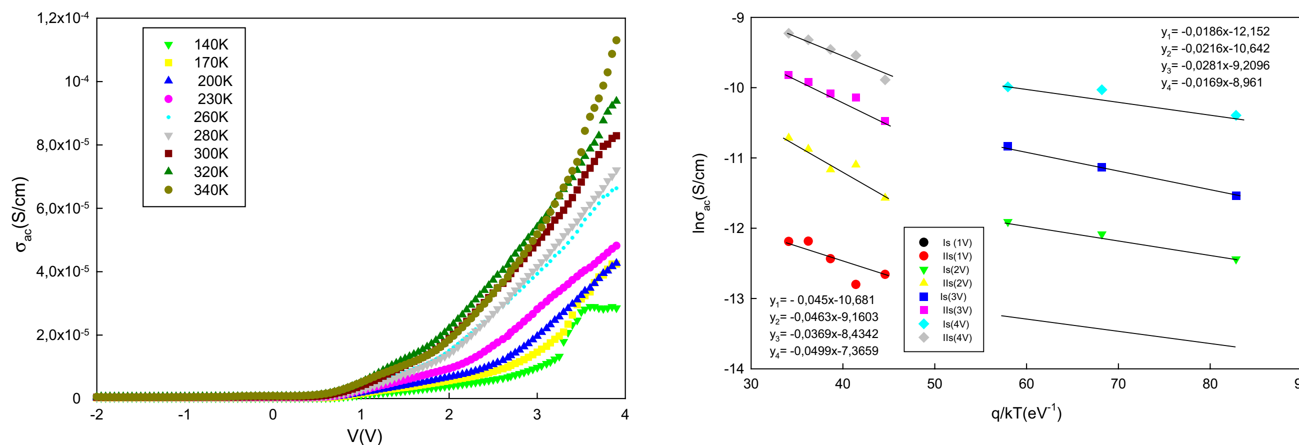

Fig. 10 Voltage dependence of the σ_{ac} at various temperature (140–340 K) for the Al/ZnS-PVA/p-Si (MPS) structure and at 500 kHz

Fig. 11 Temperature dependence of the lnσ_{ac} versus q/kT plots for various applied bias voltage of the Al/ZnS-PVA/p-Si (MPS) structure at 500 kHz

temperature regions. The obtained values of σ_0 and E_a for various applied voltages at accumulation region are tabulated in Table 2. It is clear that the value of E_a is enough high for each voltage due to the sum of energies required for the generation of the charge carriers and their motion into vacancies.

All of these experimental results show that the existence an interfacial polymer layer and surface states between metal and semiconductor, and series resistance of structure can be caused important fluctuations both in the electrical and dielectric properties [37–43]. While the temperature becomes increase, forbidden band gap of semiconductor becomes decrease and so more and more electrons can easy pass from valance band to conduction band or trap to trap and lead to the increase of conductivity. Therefore, both the electric and dielectric properties in the MIS and MPS type structures are strong function of temperature and voltage and these changes becomes more effective especially at low temperatures, but while a specially

Table 2 The obtained values of σ_0 and E_a for various applied voltage at accumulation region for various applied bias voltage

Voltage (V)	Low temperatures		High temperatures	
	σ_0 (S/cm)	E_a (meV)	σ_0 (S/cm)	E_a (meV)
1	2.30×10^{-5}	49.9	1.28×10^{-4}	16.9
2	1.05×10^{-4}	39.6	1.00×10^{-4}	28.1
3	2.17×10^{-4}	46.3	2.39×10^{-5}	21.6
4	6.32×10^{-4}	45.0	5.28×10^{-4}	18.6

density distribution of surface states are more effective in the depletion and accumulation regions, series resistance of the structure is effective only at accumulation region, respectively.

4 Conclusion

In this study, (ZnS doped PVA) nanostructures have been prepared by microwave-assisted method and its structural and morphological properties have been investigated by XRD and SEM methods. The observed three different diffraction (111), (220) and (311) peaks are corresponding to the cubic crystalline ZnS with cubic structure (*JCPDS* Data file: 05-0566-cubic). The relatively noisy behavior of the XRD pattern indicates the existence of the amorphous PVA materials inside the structure. The prepared (ZnS-PVA) nanostructure has been used as interfacial layer between Al and p-Si to prevent interfusion and reaction between of them. The temperature dependence of the electrical and dielectric properties of the fabricated Al/(ZnS-PVA)/p-Si (MPS) structures was also studied in detail in the wide range of temperature (140–340 K) and voltage (− 2 V to + 4 V) using capacitance/conductance-voltage (*C*/*G*–*V*) measurements at 500 kHz. The increase of *C* and *G* with increasing temperature was attributed to the decrease of forbidden band gap of semiconductor with increase temperature. Thus, more and more electrons can easy pass from valance band to conduction band and lead to the increase of conductivity. Contrary to the value of G or σ, the real value of R_s which is corresponding to the strong accumulation region decrease with increasing temperature. Similarly, the dielectric parameters are also found a strong function of temperature and voltage. While the values of ε', ε'' and tanδ increase with increasing temperature, the values of σac, M' and M'' decrease. The observed two linear regions with different slopes for various applied bias voltages in the Arrhenius plot ($ln(\sigma ac)$ vs. q/kT) show that the existence two different conduction mechanisms which are corresponding to the low (140–230 K) and high (260–340 K) temperatures. The value of activation energy (E_a) are found from the slope of these plots for two regions and its value for high temperatures is found lower than low temperatures due to gain enough thermal energy, thermal velocity and shrinking band gap of semiconductor. These experimental results show that the existence an interfacial polymer layer and surface states between metal and semiconductor, and series resistance of structure can be caused important fluctuations both in the electrical and dielectric properties.

Acknowledgements This study was supported by Gazi University Scientific Research Project. (Project Number: GU-BAP.05/2018-10).

References

1. İ Yücedağ, Optoelectron. and Adv. Mater. Rapid Commun. **3**, 612 (2009)
2. N.B. Ukah, D. Adil, J. Granstrom, R.K. Gupta, K. Ghosh, S. Guha, Org. Electron. **12**, 1580–1587 (2011)
3. S.M. Sze, *Physics of Semiconductor Devices*, 2nd edn., (Wiley, New York, 1981)
4. A. Tataroğlu, İ Yücedağ, Ş. Altındal, Microelectron. Eng. **85**, 1518–1523 (2008)
5. M. Sharma, S.K. Tripathi, Mater. Sci. Semicond. Process. **41**, 155–161 (2016)
6. İ. Yücedağ, A. Kaya, Ş. Altindal, Int. J. Modern Phys. B **28**, 1450153 (2014)
7. G. Aras, E. Orhan, A.B. Selçuk, S. Bilge Ocak, M. Ertuğrul, Procedia Soc. Behav. Sci. **195**, 1740–1745 (2015)
8. G. Ersöz, İ. Yücedağ, Y. Azizian-Kalandaragh, İ. Orak, Ş. Altındal, IEEE Trans. Electron. Dev. **63**, 2948–2955 (2016)
9. N. Baraz, İ. Yücedağ, Y. Azizian-Kalandaragh, G. Ersöz, İ. Orak, Ş. Altındal, B. Akbari, H. Akbari, J. Electron. Mater. **46**, 4276–4286 (2017)
10. Y. Asar, T. Asar, Ş Altındal, S. Özçelik, Philos. Mag. **95**, 2885–2898 (2015)
11. S.A. Yerişkin., M. Balbaşı, A. Tataroğlu, J. Appl. Polym. Sci. **133**, 145–151 (2016)
12. N.K. Farhana, M.H. Khanmirzaei, S. Ramesh, J. App. Polym. Sci. **134**, 45091–45097 (2017)
13. M.M. Bülbül, S. Zeyrek, S. Altındal, H. Yüzer, Microelectron. Eng. **83**, 577–581 (2006)
14. B. Elaydy, M. Hafez, Bull. Mater. Sci. **33**, 149–155 (2010)
15. M. Gökçen, T. Tunç, S. Altındal, I. Uslu, Cur. App. Phys. **12**, 525–530 (2012)
16. L. Vafayi, S. Gharibe, S. Afshar, J. Appl. Chem. Res. **7**, 63 (2013)
17. E.K. Goharshadi, S.H. Sajjadi, R. Mehrkhah, P. Nancarrow, Chem. Eng. J. **209**, 113 (2012)
18. H.V. Chung, P.T. Huy, T.T. An, N.T.M. Thuy, N.D. Chien, J. Korean Phys. Soc. **52**, 1562 (2008)
19. M. Dela Garza, I. Lopez, F. Avina, I. Gomez, J. Ovonic Res. **9**, 89 (2013)
20. T. Prakash, R. Jayaprakash, G. Neri, S. Kumar, J. Nanopart. **2103**, 1 (2013)
21. N. Baraz, İ Yücedağ, Y. Azizian-Kalandaragh, Ş Altındal, J. Mater. Sci.: Mater. Electron. **28**, 1315–1321 (2017)
22. İ Yucedağ, A. Kaya, H. Tecimer, Ş Altındal, Mater. Sci. Semicond. Process. **28**, 37–42 (2014)
23. H.P. Klug, L.E. Alexander, *X-ray Diffraction Procedures*, 2nd edn. (Wiley, NewYork, 1964)
24. S. Demirezen, Appl. Phys. A **112**, 827–833 (2013)
25. T. Tunç, M. Gökçen, I. Uslu, Appl. Phys. A **109**, 649–653 (2012)
26. K. Ozga, J. Michel, B.D. Nechyporuk, J. Ebothé, I.V. Kityk, A.A. Albassam, A.M. El-Naggar, A.O. Fedorchuk, Phys. E **81**, 281–289 (2016)
27. K. Qiu, D. Qiu, L. Cai, S. Li, W. Wu, Z. Liang, H. Shen, Mater. Lett. **198**, 23–26 (2017)
28. E.H. Nicollian, J.R. Brews, *MOS Physics And Technology* (Wiley, New York, 1982)
29. S.A. Awan, R.D. Gould, Thin Solid Films **423**, 267–272 (2003)
30. S. Demirezen, A. Kaya, S.A. Yeriskin, M. Balbası, I. Uslu, Results Phys. **6**, 180–186 (2016)
31. A.A. Sattar, S.A. Rahman, Phys. Status Solid. A **200**, 415–422 (2003)
32. A. Cherif, S. Jomni, H. Saghrouni, W. Belgacem, K. Khirounic, L. Beji, J. Alloys Compd. **685**, 28–33 (2016)
33. S. Hlali, A. Farji, N. Hizem, L. Militaru, A. Kalboussi, A. Souifi, J. Alloys Compd. **713**, 194–203 (2017)

34. H. Saghrouni, S. Jomni, W. Belgacem, N. Elghoul, L. Beji, Mat. Sci. Semi. Process. **29**, 307–314 (2015)
35. N. Shiwakoti, A. Bobby, K. Asokan, B. Antony, Mater. Sci. Semicond. Process. **42**, 378–382 (2016)
36. ÇS. Güçlü, A.F. Özdemir, A. Kökce, S. Altindal, Acta Phys. Pol. A **130**, 325–330 (2016)
37. A. Buyukbas, A. Tataroglu, M. Balbaşı, J. Optoelectron. Adv. Mater. **17**, 1134–1138 (2015)
38. Ç. Bilkan, Y. Azizian-Kalandaragh, Ş Altındal, R.S. Havigh, Phys. B **500**, 154–160 (2016)
39. E.E. Tanrıkulu, S. Demirezen, Ş Altındal, İ Uslu, J. Mater. Sci.: Mater. Electron. **29**, 2890–2898 (2018)
40. S. Altındal Yerişkin, M. Balbaşı, İ Orak, J. Mater. Sci.: Mater. Electron. **28**, 14040–14048 (2017)
41. İ Taşçıoğlu, Ö Tüzün Özmen, H.M. Şağban, E. Yağlıoğlu, Ş Altındal, J. Electron. Mater. **46**, 2379–2386 (2017)
42. Z. Wang, W. Zhou, L. Dong, X. Sui, H. Cai, J. Zuo, Q. Chen, J. Alloys Compd. **682**, 738–745 (2016)
43. S. Amrin, V.D. Deshpande, Physica E **87**, 317–326 (2017)